Origin of Enhancement in Open-Circuit Voltage by Adding ZnO to Nanocrystalline SnO_2 in Dye-Sensitized Solar Cells

Daisuke Niinobe, Yuki Makari, Takayuki Kitamura, Yuji Wada,* and Shozo Yanagida

Department of Material and Life Science, Graduate School of Engineering, Osaka University, 2-1 Yamadaoka, Osaka 565-0871, Japan

Received: April 6, 2005; In Final Form: June 3, 2005

SnO_2 + ZnO working electrodes for dye-sensitized solar cells were made by mixing a nanocrystalline SnO_2 colloidal dispersion with ZnO or $Zn(CH_3COO)_2$. Addition of ZnO or $Zn(CH_3COO)_2$ enhanced the open-circuit voltage (V_{oc}) of the cells with respect to cells containing only SnO_2. Dependence of the electron lifetime in the electrodes on short-circuit photocurrent density (J_{sc}) gave evidence against the assumption that the suppression of back electron transfer to the electrolyte is the origin for the V_{oc} enhancement by addition of Zn. V_{oc} dependence on temperatures indicated a decrease in the combined capacitance of the mixed electrode. The slope of the V_{oc} dependence versus the logarithm of J_{sc} indicated that the contribution of unpinning of the band to the enhancement of V_{oc} could be neglected. From the cyclic voltammograms of the electrodes, the combined capacitance of the mixed electrode was 1 order of magnitude smaller than that of SnO_2. The decrease in the combined capacitance in the mixed electrode could be explained by the decrease in the chemical capacitance of SnO_2, thus the shift of the conduction band position toward the vacuum level. X-ray photoelectron spectra of Sn $3d_{5/2}$ peaks showed a shift toward lower binding energy with an increasing amount of added Zn. This was attributed to an increase in the surface potential toward the negative direction, which might have resulted from a dipole moment formed by Zn on the surface of SnO_2.

1. Introduction

Recently, exhaustion of energy resources and greenhouse effects have been drawing much attention due to the rapidly growing consumption of fossil fuels. Solar cells will therefore play an important role in overcoming these problems. However, the cost of power generation by solar cells is still much higher than those of conventional power generation methods. Therefore, it is necessary for commercialization of solar cells to improve their energy conversion efficiency and bring down the production cost.

Dye-sensitized solar cells (DSSCs) are one of the most promising candidates for large-scale use among photovoltaics because of their potential for manufacture at a low cost.[1,2] Their working electrodes are usually made up of semiconductor nanoparticles, such as TiO_2, which is a very cheap material generally used as a pigment. Their light-absorption layers are usually made up of a ruthenium dye adsorbed on the semiconductor particles as a monolayer,[2,3] which could be replaced by cheap organic dyes. Furthermore, DSSCs would have great advantages as third-generation photovoltaics[4] due to the following reason. An approach for third-generation photovoltaics is to introduce a multiple-band structure by fabricating a heterointerface, which can be seen in quantum well solar cells[5,6] and would be needed in quantum dot solar cells.[7] A problem to be solved in multiple-band structure is the large recombination loss via the recombination center induced by the heterointerface. However, in DSSCs, because negative and positive carriers are present and transported in the different phases, the influence of loss by such a recombination center can be lowered.[8] However, the conversion efficiencies of present DSSCs are insufficient for commercialization in comparison with conventional Si counterparts so far. Because energy conversion efficiency influences directly the cost of electric power generation, this drawback in efficiency is disadvantageous for power generation cost, impeding practical application.

Since Tennakone et al. have achieved a dramatic enhancement in the conversion efficiency of DSSCs with SnO_2 by applying mixed SnO_2 and ZnO semiconductor particles (SnO_2 + ZnO) to the working electrode,[9] a new approach to improving the conversion efficiency of DSSCs has been opened, and several combinations of mixed semiconductor electrodes were examined, i.e., SnO_2 + Y_2O_3, SnO_2 + ZrO_2, and SnO_2 + TiO_2.[10] However, the mechanism of enhancement has not been fully understood yet. Revelation of the enhancement mechanism will lead to further improvement of conversion efficiency and furthermore may contribute to the progress of third-generation photovoltaics using DSSCs. Since the cells with SnO_2 + ZnO electrodes showed the largest enhancement of V_{oc} among the other mixed oxide electrodes and its conversion efficiency was about 8%, which is comparable to a cell with a TiO_2 electrode, we have focused on studying the origin of the enhancement in the SnO_2 + ZnO electrode. Because the improvement in mixed oxide electrodes in current−voltage ($I-V$) characteristics mainly appeared in open-circuit voltage (V_{oc}),[10−14] the main question has been concentrated on how the V_{oc} enhancement can be achieved. It has been widely assumed for the SnO_2 + ZnO electrodes that the improvement arises from the suppression of back electron transfer from the semiconductor by the core−shell structure in which a shell material with a higher conduction band (CB) energy would work as a potential barrier[10,11,15] against the carrier recombination (Figure 1b). In this mechanism, the quasi-Fermi level of the electrode would shift toward the vacuum level by elongation of the electron lifetime in the

* Author to whom correspondence should be addressed. E-mail: ywada@mls.eng.osaka-u.ac.jp.

10.1021/jp051753g CCC: $30.25
Published on Web 09/07/2005

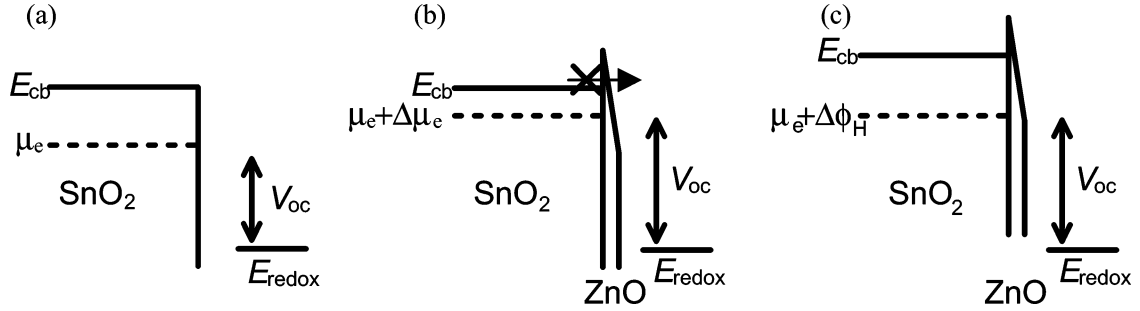

Figure 1. (a) Proposed mechanisms for enhancement of V_{oc} in SnO_2 + ZnO mixed electrodes with respect to an electrode containing only SnO_2; (b) the shift of the chemical potential of the electrons in the electrode by suppression of back electron transfer; (c) the shift of the CB edge by an increase in surface potential or the unpinning of bands. Broken lines represent the energy position of the quasi-Fermi level of electrons in the electrodes, μ_e represents the chemical potential of electrons in the electrodes, $\Delta\mu_e$ represents the shift of the chemical potential by suppression of back electron transfer, $\Delta\phi_H$ represents the amount of potential shift in the Helmholtz layer, E_{CB} is the position of the conduction band edge, and E_{redox} is the redox potential of the electrolyte.

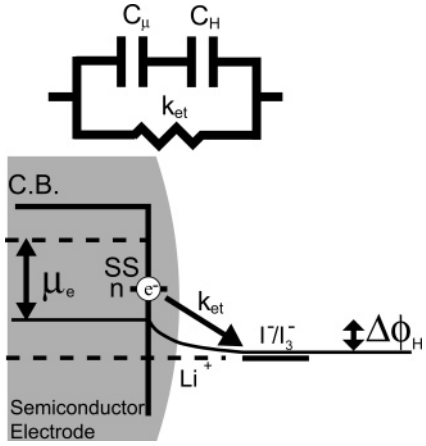

Figure 2. Model and the equivalent circuit considered here. In this model, there are electron reservoirs of chemical capacitance,[18] C_μ, and Helmholtz capacitance, C_H, of the semiconductor electrode. The electron density in these capacitors is denoted as n. These electrons recombine with I_3^- in the electrolyte with kinetic constants k_{et}. μ_e denotes the difference in chemical potential between the electrode and the electrolyte at the operative condition, and ϕ_H denotes the potential difference in the Helmholtz layer. SS denotes the surface trap states of the semiconductor nanoparticles.

electrodes. However, the shift of the conduction band position toward the vacuum level (Figure 1c)[13,16,17] must also be taken into account in such a structure.

In this report, we investigated the origin of the V_{oc} enhancement induced by addition of ZnO to SnO_2 for the working electrode. We showed the dependence of V_{oc} on log J_{sc} and temperature and V_{oc} decay kinetics to study the origin in the operative condition. The shift of the CB edge position is proposed as the origin of the enhancement of V_{oc} rather than suppression of back electron transfer from SnO_2.

2. Model and Theoritical Expression for Behaviors of V_{oc}

We use a simple model where electron reservoirs in surface states of the semiconductor particles for the chemical potential and electric potential are in parallel with a Faradaic resistance.[19−23] The model and the equivalent circuit considered here are shown in Figure 2. The possible reasons for the V_{oc} enhancement in this model can be classified into three factors as follows.

Case 1. The shift of the chemical potential of electrons in the electrode is caused by the suppression of back electron transfer from the electrode to the electrolyte by a barrier against tunneling of electrons[10] (Figure 1b). The suppression of back electron transfer decreases k_{et}, therefore elongating the electron lifetime.

Case 2. The shift of the CB edge is caused by an increase in the surface potential induced by surface adsorbate (Figure 1c). For example, it is well-known that 4-*tert*-butylpyridine in the electrolyte enhances V_{oc} of DSSCs.[19]

Case 3. The shift of the CB edge of the semiconductor electrode at the operative condition could be induced by the electric potential of electrons in surface trap states (Figure 1c). This is usually denoted as band unpinning.[24,25] Cases 2 and 3 can be expressed as a decrease in the combined capacitance because the negative shift of the CB is equivalent to the decrease in the chemical capacitance.

The contributions of these effects to V_{oc} are formulated in the following. When only a capacitance C_μ is taken into account, V_{oc} can be denoted as (Appendix A)

$$V_{oc} = \frac{2(E_{CB} - E_{redox})}{q} + \frac{kT}{q\alpha\beta} \ln \frac{J_{sc}}{\eta q d (1-P) k_{et} n_{ox} N_L^{\beta} N_c^{\alpha\beta}} \quad (1)$$

Here, it should be noted that the change in n_{ox} by the change in J_{sc} can be neglected because the amount of redox couple in the electrolyte with ordinal composition is high enough with respect to the amount of electrons in the electrode to keep the redox potential constant. Therefore, we use the redox potential of I^-/I^-_3 as the reference of potential. In case 1, the kinetic constant for back electron transfer, k_{et}, is decreased by the barrier induced by a shell material. In this case, the tunneling current from semiconductor particles to the oxidized species in the electrolyte would be decreased by the factor $\exp(-\chi^{\delta/2})$, where χ is an offset of the CB edge between a shell and a core semiconductor and δ is the shell thickness (Å).[26,27] Therefore, eq 1 would become

$$V_{oc} = \frac{kT\chi^{\delta/2}}{q\alpha\beta} + \frac{2(E_{CB} - E_{redox})}{q} + \frac{kT}{q\alpha\beta} \ln \frac{J_{sc}}{\eta q d (1-P) k_{et} n_{ox} N_L^{\beta} N_c^{\alpha\beta}} \quad (2)$$

In case 2, E_{CB} in eq 1 is increased, and therefore V_{oc} would be enhanced. In case 3, the effect of the Helmholtz capacitance, C_H, should be taken into account. Under an approximation that the density of surface states is constant through the band gap, the change in the electric potential in the Helmholtz layer, i.e., the amount of shift of the CB, ΔV_{CB}, is depicted as[25]

$$\Delta V_{CB} = \frac{kTD_{ss}}{C_H} \ln\left(1 + \frac{J_{sc}}{q k_{et} n_{ox} n_{s0}}\right) \quad (3)$$

where D_{ss} is the density of surface states per unit potential. Therefore, V_{oc} would be depicted as

$$V_{oc} = \frac{kTD_{ss}}{C_H} \ln\left(1 + \frac{J_{sc}}{qk_{et}n_{ox}n_{s0}}\right) + \frac{2(E_{CB} - E_{redox})}{q} + \frac{kT}{q\alpha\beta} \ln \frac{J_{sc}}{\eta qd(1-P)k_{et}n_{ox}N_L^{\beta}N_c^{\alpha\beta}} \quad (4)$$

Here, it should be noted that the first term in eq 4 can be attributed to the difference in the electric potential in the Helmholtz layer, and the combination of the second and third term can be attributed to the chemical potential stored in the chemical capacitance.

The possible reasons mentioned above for the V_{oc} enhancement would cause different behaviors in V_{oc} dependence on log J_{sc} and temperature. The behaviors can be simulated by the equations expressed above. In the case of suppresion of back electron transfer, V_{oc} dependence on log J_{sc} would shift toward the *y*-axis without a change in the slope. This behavior can be seen in the literature,[17] where V_{oc} increased with decreasing I_3^- concentration without a definite change in the slope in V_{oc} dependence on irradiation light intentsity. In this case, the slope of V_{oc} dependence on temperature would be decreased toward the positive direction by suppresion of back electron transfer. In the case of the shift of the CB, i.e., case 2, the plot of V_{oc} dependence versus log J_{sc} would shift toward the *y*-axis without a change in the slope, and the V_{oc} dependence on temperature would also shift toward the *y*-axis without a change in the slope. In case 3, eq 4 indicates that the slope of the V_{oc} dependence versus log J_{sc} becomes much larger[19,24] with respect to the no unpinning condition because the slope is represented as kT ln $10/q(1/(\alpha\beta) + qD_{ss}/C_H)$. The V_{oc} dependence on temperature would show a shift toward the *y*-axis by a shift of the conduction band in this case.

3. Experimental Section

The cell fabrication processes can be referred to in the literature.[28] ZnO powder (Aldrich, $\phi < 1$ μm) or $Zn(CH_3COO)_2$ (Aldrich) was mixed with 15 wt % SnO_2 colloidal dispersion (Alfa Aesar) in a mortar to result in a concentration of ZnO of 53 wt % and that of $Zn(CH_3COO)_2$ of 4, 8, and 30 mol %, with respect to SnO_2 respectively. Hereafter, we denote these samples as 53 wt % ZnO, 4 mol % $Zn(CH_3COO)_2$, 8 mol % $Zn(CH_3COO)_2$, and 30 mol % $Zn(CH_3COO)_2$, respectively. Pure SnO_2 and ZnO electrodes were also prepared as described previously.[28] We simply denote the cells with these electrodes as SnO_2 and ZnO, respectively. These were then mixed with 0.1 mL of CH_3COOH, 0.1 mL of 2,4-pentandione, 120 mg of Marporose 60MP-50 (Matsumoto Yushi Seiyaku), and 0.1 mL of Triton X-100. The resulting pastes were spread on fluorine-doped tin-oxide-coated glass substrates (FTO, Nippon Sheet Glass, <8 Ω/cm) with a squeegee and a spacing tape to make films. These electrodes were sintered in a furnance at 450 °C for 30 min, resulting in conversion of the added Zn species to ZnO. The electrodes were then dipped into an acetonitrile and *tert*-butyl alcohol solution (1:1) containing 3×10^{-4} mol/L *cis*-di(thiocyanato)-*N*,*N*′-bis(2,2-bipyridyl-4-carboxylate-4-tetrabutylammonium carboxylate) ruthenium(II) (Ru535, Solalonix) dye for 10 h. These electrodes were assembled to make solar cells by sandwiching the above dye-coated electrodes with Pt sputtered FTO electrodes and introducing the methoxyacetonitrile electrolyte containing 0.1 M LiI, 0.05 M I_2, 0.5 M 4-*tert*-butylpyridine, and 0.6 M 1,2-dimethyl-3-propylimidazolium iodide redox species. These cells were sealed by Himilan (Mitsui-Dupont Polychemicals). Measurements of current−voltage ($I-V$) characteristics of these fabricated cells were carried out under the irradiance of 100 mW/cm^2 (AM 1.5) with a simulated solar light source (Yamashita Denso, YSS-50A). V_{oc} dependence on log J_{sc} was measured by changing the irradiation intensity by degrading the 100 mW/cm^2 light source with an ND filter. The V_{oc} decay measurements of the cells were carried out for obtaining electron lifetimes in the working electrodes with the 100 mW/cm^2 simulated solar light.[29] Cyclic voltammograms (CVs) of the cells were measured using a BAS-100W (Bioanalytical Systems, Inc.). X-ray photoelectron spectroscopy (XPS) measurements were carried out, showing a change in the surface potential of SnO_2 with an increasing amount of Zn. For XPS measurements, the film was peeled off the substrate for measuring the powders. The XPS measurements were performed with a QuanteraSXM PHI using an Al Kα monochromatized X-ray source.

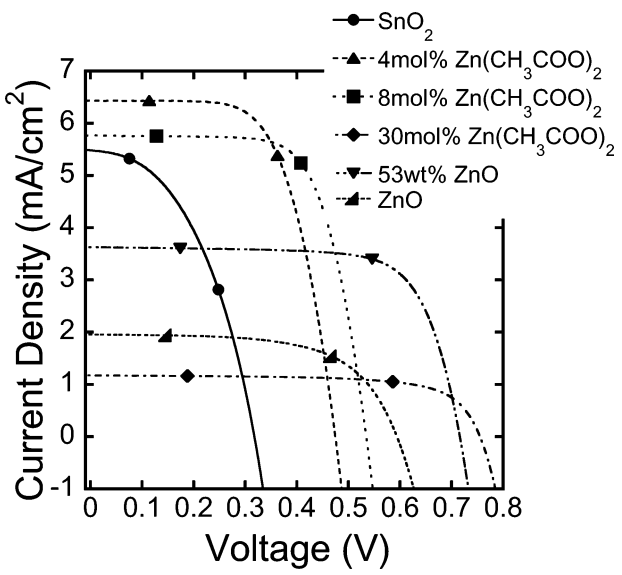

Figure 3. $I-V$ characteristics of the cells made up of SnO_2, 4 mol % $Zn(CH_3COO)_2$, 8 mol % $Zn(CH_3COO)_2$, 30 mol % $Zn(CH_3COO)_2$, 53 wt % ZnO, and ZnO electrodes under simulated AM 1.5 light. The thicknesses of the films were 2 μm.

4. Results and Discussion

4.1. $I-V$ Characteristics. The $I-V$ characteristics of the cells prepared as mentioned in the Experimental Section are shown in Figure 3. The conversion efficiencies of the cells were 0.79% (SnO_2), 2.0% (4 mol % $Zn(CH_3COO)_2$), 2.1% (8 mol % $Zn(CH_3COO)_2$), 0.87% (30 mol % $Zn(CH_3COO)_2$), 1.9% (53 wt % ZnO), and 0.72% (ZnO). The differences in J_{sc} of SnO_2, 4 mol % $Zn(CH_3COO)_2$, and 8 mol % $Zn(CH_3COO)_2$ could originate from the extent of light scattering by ZnO. The J_{sc} value of 30 mol % $Zn(CH_3COO)_2$ and 53 wt % ZnO were much smaller than those of SnO_2, 4 mol % $Zn(CH_3COO)_2$, and 8 mol % $Zn(CH_3COO)_2$. This could be attributed to the decrease in the surface area of SnO_2 and light scattering by ZnO. Especially in the case of 30 mol % $Zn(CH_3COO)_2$, J_{sc} could have been decreased because the connectivity between SnO_2 partcles became poor, with respect to SnO_2, 4 mol % $Zn(CH_3COO)_2$, and 8 mol % $Zn(CH_3COO)_2$, due to the high $Zn(CH_3COO)_2$ concentration. Another possibility is that the electron injection efficiency to the semiconductor electrode might be decreased if the CB of the electrode was shifted.

The striking enhancement of V_{oc} by increasing the ratio of $Zn(CH_3COO)_2$ to SnO_2 was observed. The highest V_{oc} was

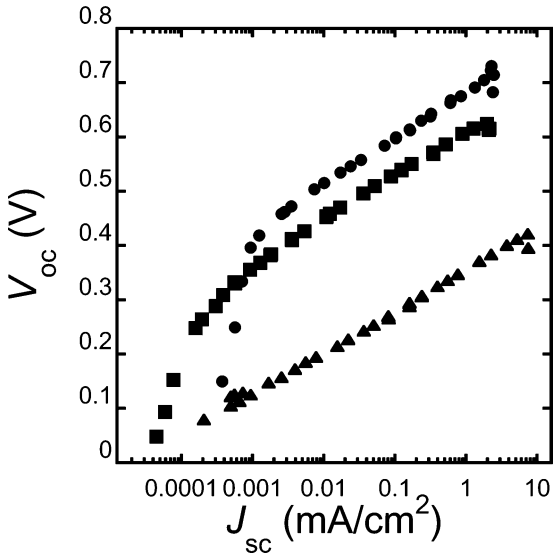

Figure 4. Relationships between V_{oc} and log J_{sc}. The electrodes were SnO_2 (triangles), ZnO (squares), and 53 wt % ZnO (circles). The thicknesses of the films were 2 μm.

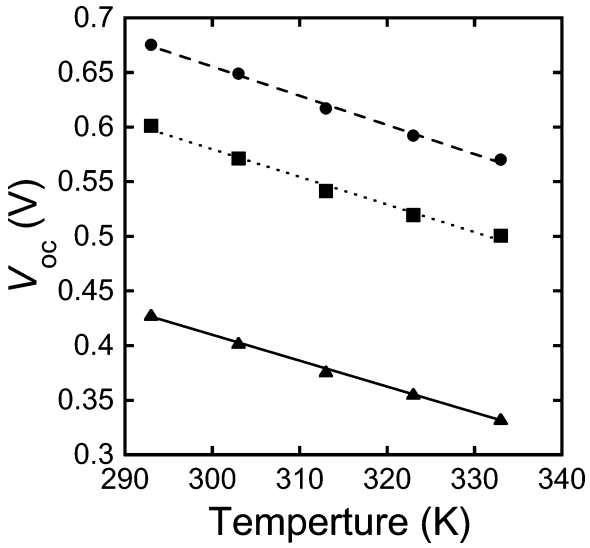

Figure 5. V_{oc} dependences of the DSSCs made up of SnO_2 (triangles), ZnO (squares), and 53 wt % ZnO (circles) on the cell temperature.

achieved for 30 mol % $Zn(CH_3COO)_2$. Here, we note that the amount of Zn in the samples of 4 mol % $Zn(CH_3COO)_2$, 8 mol % $Zn(CH_3COO)_2$, and 30 mol % $Zn(CH_3COO)_2$ correspond to 2, 4, and 18 wt % of ZnO, respectively. These amounts were less than 53 wt % ZnO, which achieved the highest efficiency among the SnO_2 + ZnO electrodes in the report by Tennakone et al.[9,30] In 4, 8, and 30 mol % $Zn(CH_3COO)_2$ samples, the thicknesses of the ZnO layers on the SnO_2 particles were estimated from the density of ZnO (5.6 g/cm^3), lattice constant of ZnO, and surface area of SnO_2 (109 m^2/g)[28] corresponding to 0.04, 0.08, and 0.3 nm, respectively. This means that the enhancement of V_{oc} by Zn was achieved by adding an amount much less than that forming a monolayer ZnO shell on the surface of the SnO_2 core particles. These results indicate that the amount of Zn^{2+} dissolved in the paste would be crucial for obtaining the V_{oc} enhancement effect.

4.2. V_{oc} Dependence on log J_{sc}. The V_{oc} dependence on log J_{sc} is shown in Figure 4. The slope of the V_{oc} dependence versus log J_{sc} shows 76 mV/decade for the SnO_2 electrode. This value equals the predicted value of kT/q = 59 mV/decade in eq 1 when $kT(dV_{oc}/d \log J_{sc})^{-1}/q$ is assumed to be 0.78, which is similar to the reported values of 0.7[31] and 0.9[17] for TiO_2 electrodes. The slopes of 53 wt % ZnO and ZnO samples are 85 and 78 mV/decade, which correspond to $kT(dV_{oc}/d \log J_{sc})^{-1}/q$ = 0.7 and 0.76, respectively, in the region of V_{oc} larger than 0.4 V. These values are almost the same as that of the SnO_2 sample. For SnO_2, 53 wt % ZnO in the region of V_{oc} > 0.4 V and ZnO in the region of V_{oc} > 0.2 V, the increase in the potential in the electrode versus the increase in light intensity should be composed of the chemical potential because the slopes in Figure 4 are similar to the reported value for TiO_2 of which bands are pinned.[19] However, the slopes of 53 wt % ZnO in the region of V_{oc} < 0.4 V and ZnO in the region of V_{oc} < 0.2 V are much larger than that of SnO_2. The slope of 53 wt % ZnO at V_{oc} < 0.4 V is 0.63 V/decade, which is about 1 order of magnitude larger than that in the region of V_{oc} > 0.4 V. To explain the larger slope in the region of V_{oc} < 0.4 V with respect to that in the region of V_{oc} > 0.4 V, decrease in the chemical capacitance, decrease in electron lifetime, unpinning of bands, and change of β must be taken into consideration because the quasi-Fermi level monotonically increases in proportion to the logarithm of the electron density.

For further discussion about the larger slope in the region V_{oc} < 0.4 V for 53 wt % ZnO and the origin of the enhancement of V_{oc} by the addition of Zn, V_{oc} dependence on temperature, V_{oc} decay measurement, and CVs were investgated in the following sections.

4.3. V_{oc} Dependence on Temperature. The V_{oc} dependences on the temperature of SnO_2, ZnO, and 53 wt % ZnO samples are shown in Figure 5. V_{oc} shows a linear dependence on temperature as predicted by eq 1. From eq 2, extrapolation of V_{oc} to T = 0 K in Figure 5 implies the position of the CB of the semiconductor relative to the redox potential of the electrolyte,[32] and the contribution of suppression of back electron transfer to the enhancement of V_{oc} would appear as the decrease in the slope in Figure 5. The slopes of SnO_2, ZnO, and 53 wt % ZnO are −23, −25, and −27 mV/K, respectively. These are the opposite results when suppression of back electron transfer is assumed in a 53 wt % ZnO sample. However, *y*-intercepts of SnO_2, ZnO, and 53 wt % ZnO are 1.1, 1.3, and 1.5 V, respectively. From these results, the enhancement of V_{oc} by adding ZnO to SnO_2 would be attributed to the shift in the CB rather than suppression of back electron transfer.

4.4. V_{oc} Decay Measurement. To investigate the influence of the addition of Zn on the back electron transfer reaction, electron lifetimes in the working electrodes were measured by the V_{oc} decay measurement method.[29] In this measurement, the lifetimes of the electrons, τ, in the electrode are estimated by the combination of the transient of open-circuit voltage and the equation[29]

$$\tau = \frac{kT}{q}\left(\frac{dV_{oc}}{dt}\right)^{-1} \quad (5)$$

In general, the electron lifetime depends exponentially on V_{oc}.[29,33] The exponential dependence of the electron lifetime on the electrode voltage could be explained by the exponential dependence of the chemical capacitance of the electrode on the potential[23] or second-order kinetics to the electron density for the back electron transfer reaction.[33]

Figure 6 shows electron lifetimes plotted versus log J_{sc}, which were obtained from the corresponding V_{oc} using the relation in Figure 4. Figure 6 shows that the electron lifetime of SnO_2 is 1 order of magnitude longer than those of 53 wt % ZnO, 4 mol % $Zn(CH_3COO)_2$, 8 mol % $Zn(CH_3COO)_2$, and 30 mol % Zn-

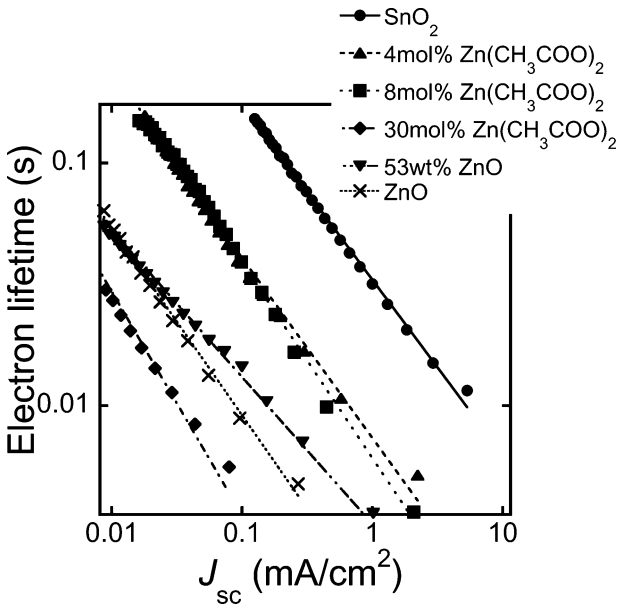

Figure 6. Electron lifetime dependences on the logarithm of J_{sc} for SnO_2, 4 mol % $Zn(CH_3COO)_2$, 8 mol % $Zn(CH_3COO)_2$, 30 mol % $Zn(CH_3COO)_2$, and 53 wt % ZnO. The plots were obtained from calculation of the transients of photovoltage.[29] The thicknesses of the films were 2 μm.

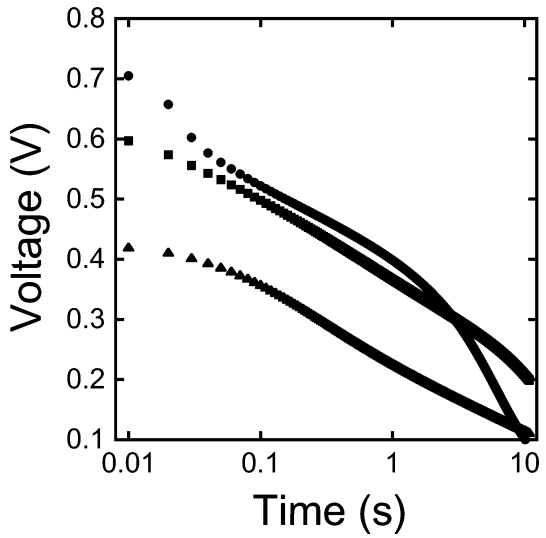

Figure 7. V_{oc} transients of the cells made up of SnO_2 (triangles), 53 wt % ZnO (circles), and ZnO (squares) plotted against a logarithmic time scale. The plots were obtained by measuring the open-circuit voltage after cutting off the irradiation of the light of AM 1.5. The thicknesses of the films were 2 μm.

$(CH_3COO)_2$. This means that the contribution of an insulating layer to lifetime elongation cannot be the cause for the enhancement of V_{oc} by adding Zn; therefore case 1 can be neglected for the origin of the enhancement of V_{oc}.

V_{oc} transients of the DSSCs in a logarithmic time scale are shown in Figure 7. The V_{oc} transients of all of the samples show a linear dependence on log t. This behavior contradicts that of a circuit consisting of a parallel combination of capacitance and ohmic resistance where voltage decays exponentially with time but is almost identical to a circuit consisting of a parallel combination of capacitance and resistance expressed by the Butler−Volmer equation. This behavior can be seen in the field of electrochemistry[34−36] and electric double-layer capacitors.[37] The V_{oc} transient for the 53 wt % ZnO sample in Figure 7 is composed of two linear parts, i.e., the early region of $t < 1$ s

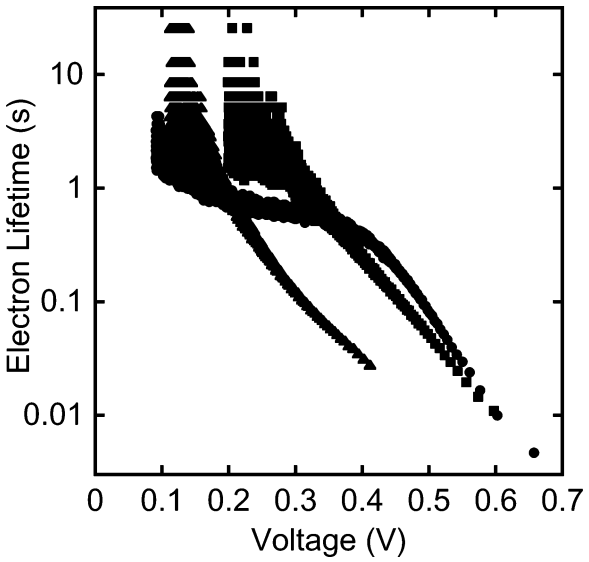

Figure 8. Electron lifetime dependences on V_{oc} of SnO_2 (triangles), 53 wt % ZnO (circles), and ZnO (squares) samples plotted in a logarithmic scale. The thicknesses of the films were 2 μm.

($V_{oc} > 0.4$ V) and the latter region of $t > 1$ s ($V_{oc} < 0.4$ V). These two linear parts correspond to the linear two parts of $V_{oc} > 0.4$ V and $V_{oc} < 0.4$ V in Figure 4, respectively; therefore, the kinetics of V_{oc} decay in the early region in Figure 7 could be attributed to the decrease in the chemical potential of the electrons in the electrode by the back electron transfer from the semiconductor to the electrolyte. However, there may be several causes for the larger slope in latter region with respect to that of early region, i.e., smaller β, relaxation of band unpinning, or a larger back electron transfer reaction. Therefore, determination of the origin of the larger slope is required to clarify the contribution of band unpinning to the increase in slope in the region $V_{oc} < 0.4$ V. β can be estimated from the equation[29]

$$\beta = 1 + \frac{d\tau}{dt} = 1 - \frac{d}{dt}\left(\frac{dV_{oc}}{d \ln t}\frac{1}{t}\right)^{-1} \quad (6)$$

In this equation, $dV_{oc}/d \ln t$ indicates the slope of V_{oc} decay plotted versus the logarithm of time. Therefore, from the slope in Figure 7, the values of β were determined to be 1.5 for SnO_2, 1.4 for ZnO in the region $t < 5$ s, 1.4 for 53 wt % ZnO in the early region, and 1.2 for 53 wt % ZnO in the latter region, respectively. In the cases of SnO_2, ZnO, and 53 wt % ZnO in the early region, β is similar to the reported value of 1.3−1.6 for the TiO_2 electrode.[38−40] However, for the 53 wt % ZnO electrode in the latter region, β is smaller than those of the other electrodes. From the β values obtained here, the increase in the slope at $V_{oc} < 0.4$ V in V_{oc} dependence on log J_{sc} by the decrease in β is estimated to be 0.03 V/decade for 53 wt % ZnO from eq 1 at most. But the observed value of the slope in the region $V_{oc} < 0.4$ V for 53 wt % ZnO in Figure 4 is 0.63 V/decade. Therefore, another contribution of 0.6 V/decade to the slope must be considered.

Figure 8 shows the electron lifetime plotted versus the V_{oc}. From the slope of the electon lifetime dependence on the V_{oc} of 53 wt % ZnO, $d \log \tau/dV_{oc}$ is estimated to be −8.2 decade/V in the region $V_{oc} > 0.4$ V and −1.0 decade/V in the region $V_{oc} < 0.4$ V. Because the ratio of the slopes in $V_{oc} > 0.4$ V and $V_{oc} < 0.4$ V is 8.2 and is the same value as that of $d \log J_{sc}/dV_{oc}$ of which the value is 8.6 when the influence of β is taken into consideration, the change in the slope in V_{oc} dependence on

log J_{sc} at $V_{oc} = 0.4$ V would be explained from the change in the slope in electron lifetime dependence on V_{oc}.

The change in d log t/dV at $V_{oc} = 0.4$ could be attributed to the change in the recombination mechanism as can be inferred from the change in β. Here, it should be noted that the recombination mechanism could be attributed to the recombination via trap states in the region $V_{oc} < 0.4$ V and from the CB through thermal excitation of trapped electrons in the region $V_{oc} > 0.4$ V, which can be inferred from Figure 8, employing the interpretation of lifetime dependence on V_{oc} by Bisquert et al.[23] From this interpretation, the lifetimes of electrons are dominated by three paths for recombination, i.e., (1) back electron transfer of free electrons from the CB, (2) the back electron transfer via surface trap states, and (3) the back electron transfer of trapped electrons via the CB. The two different regions in the lifetime dependence on V_{oc} of 53 wt % ZnO can be attributed to the back electron transfer from the CB for $V_{oc} > 0.4$ V and from surface trap states for $V_{oc} < 0.4$ V, respectively, because the curved shape at $V_{oc} < 0.4$ V could be attributed to the Gaussian shape of the density of oxidized species in electrolyte and the linear shape at $V_{oc} > 0.4$ V can be attributed to the exponential dependence of the density of excited electrons in the CB and the tailing parameter for the distribution of trap states on the potential of the electrode. The interpretation means that the surface trap states would be increased by the addition of ZnO. This is consistent with our conclusion that the changes in the slopes in Figures 4 and 7 at $V_{oc} < 0.4$V were attributed to the change in the recombination mechanism. However, the lifetime dependence on V_{oc} of SnO_2 and ZnO electrodes were almost linear. This could be attributed to the lower density of surface trap states in these electrodes with respect to 53 wt % ZnO. In the case of SnO_2, the lifetime dependence on V_{oc} shows a tendency for saturation at 0.3 V. This could be attributed to the back electron transfer from the CB without interference from the trapping and detrapping speeds of the electrons. Here, the slope of the linear part of the lifetime dependence on V_{oc} can be expressed as

$$\frac{\mathrm{d} \ln \tau}{\mathrm{d}V_{oc}} = \frac{q}{kT}(\alpha - 1) \tag{7}$$

Therefore, almost the same slopes of -9.1 and -8.2 decade/V in the linear part of the lifetime dependence on V_{oc} in SnO_2 and 53 wt % ZnO electrodes mean that the tailing parameter would not be affected by the addtion of ZnO.

Theoretical investigation by other reseachers,[42] which took the influence of back electron transfer via monoenergetic surface trap states into consideration as a recombination path, indicated that the change in the dominant recombination path from the surface states to the CB by increasing light intensity would induce a stepwise increase in electron density, which induces a curve in electron density dependence on the light intensity. This also suggests that the change in the recombination mechanism from surface states to the CB caused the change in the slope at $V_{oc} = 0.4$ V in Figure 4.

From the result above, the larger slope in the region $V_{oc} < 0.4$ V for 53 wt % ZnO would not be attributed to unpinning of the band, and from the slope in the region $V_{oc} > 0.4$ V, the band could be pinned in the region $V_{oc} > 0.4$ V as mentioned previously. Therefore, unpinning of the band, which corresponds to case 3, would not be the cause for the V_{oc} enhancement.

4.5. CV Measurements. To study the effects of the capacitance of the electrode, CVs of the cells under dark conditions were measured.

The current density observed in CVs under dark conditions is expressed as

$$i = Cs + i_F \tag{8}$$

where i is the current density observed in the CV, i_F is the Faradaic current, C is the combined capacitance of the electrode, and s is the sweep velocity. When the sweep speed is adequately fast, the current observed in the CV would be dominated by the current into/from the capacitor; therefore the Faradaic current can be neglected in eq 8. When the Faradaic current can be neglected in the model described in Figure 2, the current density in the CV measurement is proportional to the capacitance and therefore can be thought of as the magnitude of the combined capacitance at the potential. A detailed analysis of behaviors on the CVs was reported by Fabregat-Santiago et al.[22] The results of the CVs for SnO_2, ZnO, and 53 wt % ZnO are shown in Figure 9. In Figure 9, the anodic currents under negative bias were observed in all of the samples, and the currents under the opposite scan directions were almost symmetrical with respect to the x-axis. This means that the sweep speed was high enough to neglect the Faradaic current at the sweep speed in Figure 9; therefore the current in the CV can be attributed to the electron flow into/from the capacitors. To neglect the Faradaic current, the sweep speed must satisfy the condition that the duration time for a sweep must be shorter than the electron lifetime at the voltage. In this sweep condition, the current density divided by a sweep speed in Figure 9 represents the magnitude of the combined capacitance as mentioned above. Therefore, the combined capacitance of these electrodes were estimated as in Figure 10.

The equivalent circuit for a 53 wt % ZnO electrode would be a parallel combination of the capacitances of SnO_2 and ZnO because there would be both of the paths for electrons from SnO_2 and ZnO to the FTO electrode. In the parallel combination of capacitance, the combined capacitance is governed by the larger one. Therefore, it was expected that the combined capacitance of the 53 wt % ZnO electrode would be governed by that of SnO_2, of which capacitance was about 1 order of magnitude larger than that of ZnO. But Figure 10 shows that the capacitance of 53 wt % ZnO is about 1 order of magnitude smaller than that of SnO_2. This means that the combined capacitance of the SnO_2 electrode would be decreased by addtion of ZnO. Because the combined capacitance of SnO_2, ZnO, and 53 wt % ZnO electrodes would be governed by the chemical capacitance rather than the Helmholtz capacitance as mentioned previously, the chemical capacitance of SnO_2 would be decreased by the addtion of Zn. From eq 11, the extrapolation of the linear part of the log C dependence on the potential to the y-axis indicates the relative position of the CB; therefore the CB of the 53 wt % ZnO would be more negative than that of SnO_2 and ZnO. This corresponds to case 2.

The amount of electrons in the semiconductor electrode can be estimated from the integral of a current density divided by a sweep speed, i.e., $\int i/s \, \mathrm{d}V$. The charge in the electrodes was estimated from the integral of the capacitance in Figure 10. The amounts of electrons in the electrodes required for obtaining 0.3 V were estimated to be 10 μC/cm^2 for the SnO_2 electrode and 2 μC/cm^2 for the 53 wt % ZnO electrode. The difference could be caused by the decrease in the chemical capacitance of SnO_2.

4.6. XPS Measurements. Sn $3d_{5/2}$ spectra of dyed SnO_2, 4, 8, 30 mol % $Zn(CH_3COO)_2$, and 53 wt % ZnO electrodes normalized to K $2p_{3/2}$ are shown in Figure 11. Because potassium ion was contained in the SnO_2 colloidal dispersion

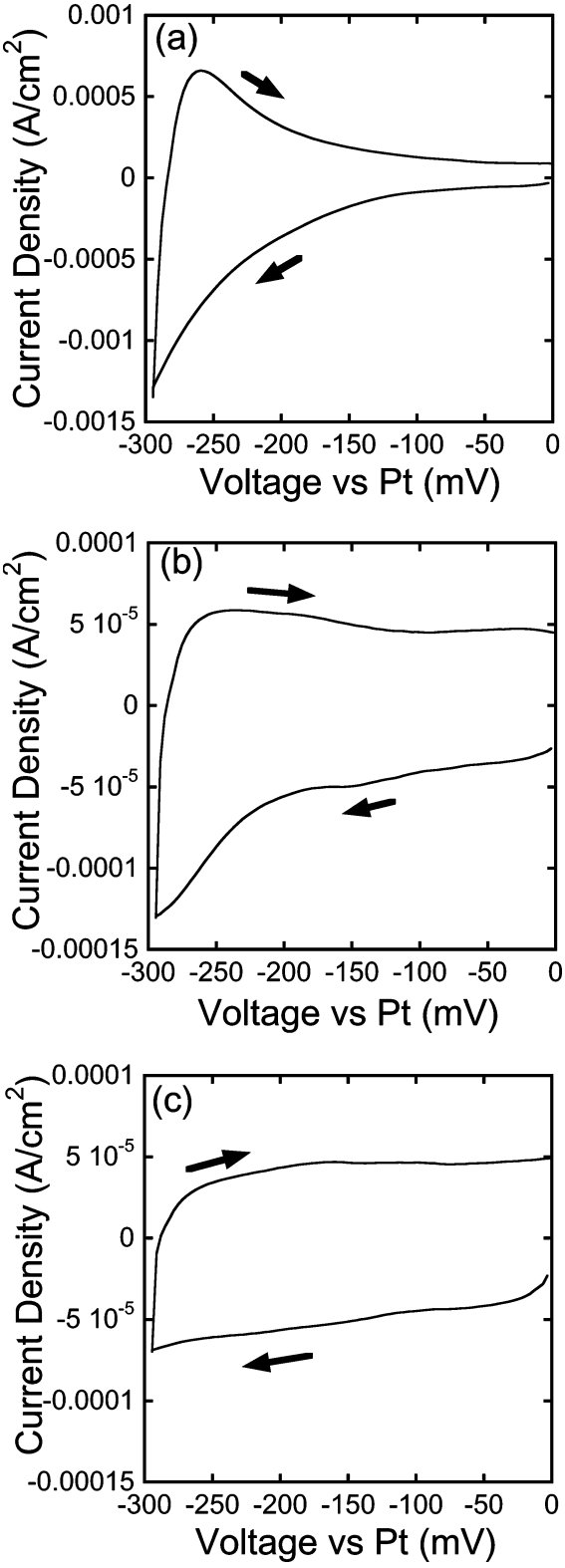

Figure 9. Cyclic voltammograms of (a) SnO_2, (b) ZnO, and (c) 53 wt % ZnO electrode under dark conditions at a sweep speed of 10 V/s. The measurements were carried out on the cells fabricated with those electrodes. The arrows indicate scan directions.

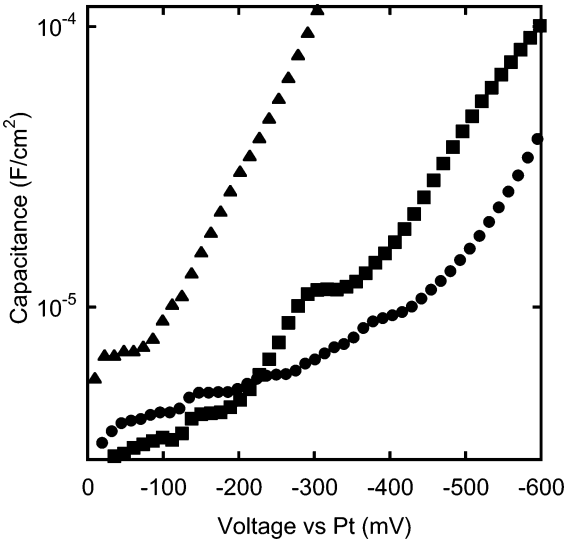

Figure 10. Estimated capacitances of SnO_2 (triangles), ZnO (squares), and 53 wt % ZnO (circles) electrodes obtained from CVs. The sweep speeds were 10 V/s.

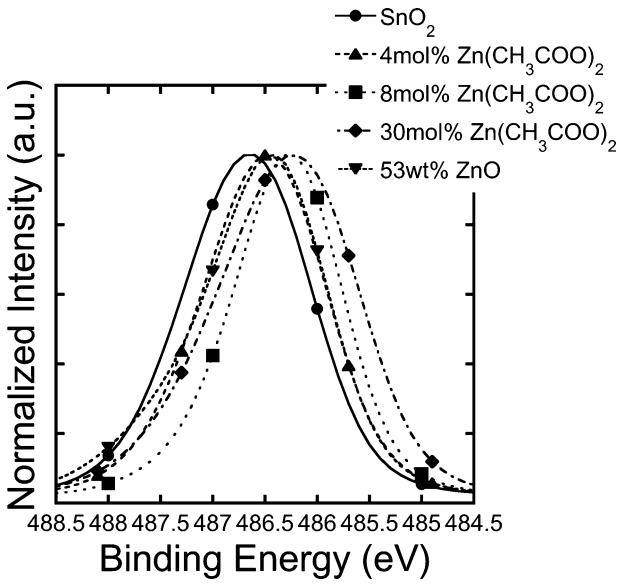

Figure 11. Sn $3d_{5/2}$ region XPS spectra of dye-coated powders peeled from the substrates. The binding energy of the spectra was normalized to K $2p_{3/2}$ for correction of charging, and the intensity was also normalized.

as a counterion, the position of the Sn $3d_{5/2}$ peak was normalized to K $2p_{3/2}$ for correction of charging. Figure 11 shows that the position of the Sn $3d_{5/2}$ peak shifted at most 0.4 eV toward lower binding energy with increasing content of Zn. The variation of Sn species would cause the surface trap states discussed previously. If the shift is caused by a chemical shift by interaction between Zn and Sn, then a peak corresponding to the interaction would appear in the spectra; therefore the shape of the peak would not be retained over such a wide range of concentrations of $Zn(CH_3COO)_2$. The peaks in Figure 11 show the entire shift with little change in the shape. Therefore, the shift of the Sn $3d_{5/2}$ peak could be attributed to the change in the surface potential.[43−45] The increase in the surface potential could be attributed to the dipole formed between Zn and Sn on the surface of SnO_2 and/or modification of the adsorption characteristics of SnO_2 by ZnO. The shift of the surface potential might also be caused by the complex formed by Zn and Ru.[46−48] This result was obtained in a vacuum, but the modification of the surface potential by Zn would be retained in the electrolyte. Although 4, 8, and 30 mol % $Zn(CH_3COO)_2$ showed an increasing amount of shift with an increasing amount of $Zn(CH_3COO)_2$, 53 wt % ZnO, which is equivalent to 68 mol % of Zn, did not show adequate shift as expected from the ZnO

concentration. This could be caused by the difference in the solubility in the solvent, therefore the concentration of Zn^{2+} in the solution.

5. Conclusions

The origin of the enhancement of V_{oc} by adding ZnO was investigated in this study. For the origin, the decrease in back electron transfer and shift of the CB were examined. We have carried out the electron lifetime measurement by open-circuit photovoltage decay measurements[29] combined with a V_{oc}−log J_{sc} plot. The results demonstrated that the V_{oc} enhancement is not caused by elongation of the electron lifetime by suppression of back electron transfer. The V_{oc} dependence on temperature has indicated that the enhancement of V_{oc} could be caused by the shift of the CB position or decrease in the chemical capacitance. From the consistency of the slope in the region $V_{oc} > 0.4$ V in V_{oc} depencence on log J_{sc} and the reported value,[17,31] the potential would be composed of the chemical potential of electrons in the electrode but not the electric potential in the Helmholtz layer. The open-circuit voltage decay measurement shows that the change in β and its influence on the enhancement of V_{oc} are negligible. The faster back electron transfer is attributed to the larger slope in the region $V_{oc} < 0.4$ V from the electron lifetime measurement. The electron lifetime dependence on V_{oc} also suggested that the back electron transfer via surface states became larger by addition of ZnO to SnO_2. CV measurements under dark conditions showed that the combined capacitance of 53 wt % ZnO was smaller than that of ZnO. This would be caused by the coating of SnO_2 by ZnO, which induces the shift of the CB of SnO_2 by modification of surface potential. XPS measurements indicated that a shift of the CB position is also caused by the electrostatic potential difference. This potential difference might be induced by specific adsorption of the dye to ZnO.

This study has shown that the enhancement of V_{oc} is mainly caused by the decrease in the chemical capacitance of the electrode by the difference in the chemical capacitance of ZnO and SnO_2.

Acknowledgment. D.N. expresses his special thanks to the center of excellence (21COE) program "Creation of Integrated EcChemistry of Osaka University".

Appendix A: An Introduction to the Relation between V_{oc} and J_{sc}

To investigate the dependence of V_{oc} on J_{sc}, we assume only one dominant recombination path of back electron transfer. The rate equation under the assumption can be depicted as

$$\frac{dn}{dt} = \frac{J_{sc}}{\eta q d(1-P)} - k_{et} n_{ox} n^{\beta} \tag{9}$$

where n is the electron density in the semiconductor electrode, t is the time, J_{sc} is the short-circuit current density, η is the electron collection efficiency, q is an electron charge, d is the thickness of the semiconductor working electrode film, P is the porosity of the film, n_{ox} is the density of oxidized species in the redox electrolyte, and β is the parameter for the order of the back electron transfer reaction. Because dn/dt equals 0 in the open-circuit condition, eq 9 can be transformed to

$$n = \left\{ \frac{J_{sc}}{\eta q d(1-P) k_{et} n_{ox}} \right\}^{1/\beta} \tag{10}$$

The generalized chemical capacitance, C_{μ}, for the semiconductor electrode is depicted as a density of states.[18,22]

$$C_{\mu} = \frac{q^2 \alpha N_L d}{kT} \exp\left(\frac{\alpha(\epsilon_e - E_c)}{kT} \right) \tag{11}$$

where N_L is the total density of states per unit volume and α is a parameter including the tailing parameter for the trap states in band gap or 1 in the case of no trap state in the band gap. The chemical capacitance shown in eq 11 could be a combined capacitance composed of several types of chemical capacitance, i.e., surface trap states, bulk trap states, and conduction band states, and the combined capacitance would mainly be governed by one of them depending on the electrode potential.[23] Therefore

$$n = \int C_{\mu}/q \, dV = N_L N_c^{\alpha} \exp\left(\frac{\alpha q V + \alpha(E_{redox} - E_{CB})}{kT} \right) \tag{12}$$

where N_c is the density of states of the CB. We define the electron density at a dark equilibrium at $V = 0$ as n_{s0}; therefore $n_{s0} = N_L N_c^{\alpha} \exp(\alpha(E_{redox} - E_{CB})/kT)$. From eqs 10 and 12, we obtain eq 1.

References and Notes

(1) O'Regan, B.; Grätzel, M. *Nature* **1991**, *353*, 737.
(2) Nazzerruddin, M. K.; Kay, A.; Podicio, I.; Humphy-Baker, R.; Muller, E.; Liska, P.; Vlachopoulos, N.; Grätzel, M. *J. Am. Chem. Soc.* **1993**, *115*, 6382.
(3) Nazeeruddin, M. K.; Zakeeruddin, S. M.; Humphry-Baker, R.; Jirousek, M.; Liska, P.; Vlachopoulos, N.; Shklover, V.; Fischer, C.-H.; Grätzel, M. *Inorg. Chem.* **1999**, *38*, 6298.
(4) Green, M. A. *Mater. Sci. Eng., B* **2000**, *74*, 118−124.
(5) Barnham, K. W. J.; Duggan, G. *J. Appl. Phys.* **1990**, *67*, 3490−3493.
(6) Barnham, K. W. J.; Ballard, I.; Barnes, J.; Connolly, J.; Griffin, P.; Kluftinger, B.; Nelson, J.; Tsui, E.; Zachariou, A. *Appl. Surf. Sci.* **1997**, *113*−*114*, 722−733.
(7) Aroutiounian, V.; Petrosyan, S.; Khachatryan, A.; Touryanb, K. J. *Appl. Phys.* **2001**, *89*, 2268.
(8) Matsumura, M.; Matsudaira, S.; Tsubomura, H. *Bull. Chem. Soc. Jpn.* **1979**, *52*, 1559.
(9) Tennakone, K.; Kumara, G. R. R. A.; Kottegoda, I. R. M.; Perera, V. P. S. *Chem. Commun.* **1999**, 15.
(10) Kay, A.; Grätzel, M. *Chem. Mater.* **2002**, *14*, 2930.
(11) Zaban, A.; Chen, S. G.; Chappela, S.; Gregg, B. A. *Chem. Commun.* **2000**, 2231.
(12) Chen, S. G.; Chappel, S.; Diamant, Y.; Zaban, A. *Chem. Mater.* **2001**, *13*, 4629.
(13) Palomares, E.; Clifford, J. N.; Haque, S. A.; Lutz, T.; Durrant, J. R. *J. Am. Chem. Soc.* **2003**, *125*, 475.
(14) Diamant, Y.; Chappel, S.; Chen, S. G.; Melamed, O.; Zaban, A. *Coord. Chem. Rev.* **2004**, *248*, 1271.
(15) Tennakone, K.; Bandaranayake, P. K. M.; Jayaweera, P. V. V.; Konno, A.; Kumara, G. R. R. A. *Physica E* **2002**, *14*, 190.
(16) Diamant, Y.; Chen, S. G.; Melamed, O.; Zaban, A. *J. Phys. Chem. B* **2003**, *107*, 1977.
(17) Liu, Y.; Hagfeldt, A.; Xiao, X.-R.; Lindquist, S.-E. *Sol. Energy Mater. Sol. Cells* **1998**, *55*, 267.
(18) Bisquert, J. *Phys. Chem. Chem. Phys.* **2003**, *5*, 5360.
(19) Schlichthörl, G.; Huang, S. Y.; Sprague, J.; Frank, A. J. *J. Phys. Chem. B 101*, 8141.
(20) van de Lagemaat, J.; Park, N.-G.; Frank, A. J. *J. Phys. Chem. B.* **2000**, *104*, 2044.
(21) Bisquert, J.; Zaban, A. *Appl. Phys. A* **2003**, *77*, 507.
(22) Fabregat-Santiago, F.; Mora-Seró, I.; Garcia-Belmonte, G.; Bisquert, J. *J. Phys. Chem. B* **2003**, *107*, 758.
(23) Bisquert, J.; Zaban, A.; Greenshtein, M.; Mora-Seró, I. *J. Am. Chem. Soc.* **2004**, *126*, 13550.
(24) Kelly, J. J.; Memming, R. *J. Electrochem. Soc.* **1982**, *129*, 730.
(25) Mao, D.; Kim, K.-J.; Frank, A. J. *J. Electrochem. Soc.* **1995**, *142*, 1869.
(26) Card, H. C.; Rhoderick, E. H. *J. Phys. D: Appl. Phys.* **1971**, *4*, 1589.
(27) Lillington, D. R.; Townsend, W. G. *Phys. Rev. Lett.* **1976**, *28*, 97.
(28) Ito, S.; Makari, Y.; Kitamura, T.; Wada, Y.; Yanagida, S. *J. Mater. Chem.* **2004**, *14*, 385.

(29) Zaban, A.; Greenshtein, M.; Bisquert, J. *ChemPhysChem* **2003**, *4*, 859.
(30) Tennakone, K.; Kottegoda, I. R. M.; Silva, L. A. A. D.; Perera, V. P. S. *Semicond. Sci. Technol.* **1999**, *14*, 975.
(31) Huang, S. Y.; Schlichthorl, G.; Nozik, A. J.; Gratzel, M.; Frank, A. J. *J. Phys. Chem. B* **1997**, *101*, 2576−2582.
(32) Kron, G.; Egerter, T.; Werner, J. H.; Rau, U. *J. Phys. Chem. B* **2003**, *107*, 3556−3564.
(33) Duffy, N. W.; Peter, L. M.; Rajapakse, R. M. G.; Wijayantha, K. G. U. *J. Phys. Chem. B* **2000**, *104*, 8916.
(34) Teak, B. V.; Conway, B. E. *Electrochim. Acta* **1976**, *21*, 745.
(35) Teak, B. V.; Rader, C. G.; Conway, B. E. *Electrochim. Acta* **1977**, *22*, 1167.
(36) Janssen, L. J. J.; Visser, G. J.; Barendrecht, E. *Electrochim. Acta* **1979**, *25*, 641.
(37) Conway, B. *Electrochemical Supercapacitors: Scientific Fundamentals and Technological Applications*; Plenum Publishers: New York, 1999; Chapter 18.
(38) Nelson, J. *Phys. Rev. B* **1999**, *59*, 15374.
(39) Fisher, A. C.; Peter, L. M.; Ponomarev, E. A.; Walker, A. B.; Wijayantha, K. G. U. *J. Phys. Chem. B* **2000**, *104*, 949.
(40) Könenkamp, R. *Phys. Rev. B* **2000**, *61*, 11057.
(41) Cameron, P. J.; Peter, L. M.; Hore, S. *J. Phys. Chem. B* **2005**, *109*, 930.
(42) Bisquert, J.; Zaban, A.; Salvador, P. *J. Phys. Chem. B* **2002**, *106*, 8774.
(43) Mullins, W.; Averbach, B. *Surf. Sci.* **1988**, *206*, 41.
(44) Ishii, H.; Sugiyama, K.; Ito, E.; Seki, K. *Adv. Mater.* **1999**, *11*, 605.
(45) Woodruff, D. P.; Delchar, T. *Modern Techniques of Surface Science*; Cambridge University Press: Cambridge, U.K., 1986; Chapter 7.
(46) Westermark, K.; Rensmo, H.; Siegbahn, H.; Keis, K.; Hagfeldt, A.; Ojamäe, L.; Persson, P. *J. Phys. Chem. B* **2002**, *106*, 10102.
(47) Keis, K.; Bauer, C.; Boschloo, G.; Hagfeldt, A.; Westermark, K.; Rensmob, H.; Siegbahn, H. *J. Photochem. Photobiol., A* **2002**, *148*, 57.
(48) Sun, C.; Berg, J. C. *Adv. Colloid Interface Sci.* **2003**, *106*, 151.